

A novel metric for assessing climatological surface habitability

Hannah L. Woodward^{1,2*}, Andrew J. Rushby^{1,2} and
Nathan J. Mayne³

¹School of Natural Sciences, Birkbeck, University of London, Malet Street, London, WC1E 7HX, Greater London, United Kingdom.

²Centre for Planetary Sciences, University College London, Gower Street, London, WC1E 6BT, Greater London, United Kingdom.

³Department of Physics and Astronomy, University of Exeter, Stocker Road, Exeter, EX4 4SB, Devon, United Kingdom.

*Corresponding author(s). E-mail(s): hannah.woodward@bbk.ac.uk;
Contributing authors: a.rushby@bbk.ac.uk; n.j.mayne@exeter.ac.uk;

Abstract

Planetary surface habitability has so far been, in the main, considered in its entirety. The increasing popularity of 3D modelling studies of (exo)planetary climate has highlighted the need for a more nuanced understanding of surface habitability. Using satellite-derived data of photosynthetic life to represent the observed surface habitability of modern Earth, we validate a set of climatologically-defined metrics previously used in exoplanetary habitability studies. The comparison finds that the metrics defined by temperature show spatial patterns of habitability distinct to those defined by aridity, with no metric able to completely replicate the observed. We build upon these results to introduce a new metric defined by the observed thermal limits of modern Earth-based life, along with surface water fluxes as an analogue for water and nutrient availability. Furthermore, we pay attention to not only the thermal bounds of macroscopic complex life, but additionally the limits of microbial life which have been vital to the generation of Earth's own biosignatures, thus expanding considerations of climatic habitability out of a historically binary definition. Repeating the validation for our metric finds a significant improvement in the spatial representation of habitability, laying the groundwork for more accurate assessments of potential life-supporting environments upon other planets.

Keywords: astrobiology, Earth, exoplanets, planets and satellites: terrestrial planets, planets and satellites: atmospheres

1 Introduction

Habitability has been investigated across many spatial and temporal scales, from the *Galactic Habitable Zone* [1, 2] to the ecological niches of extremophiles [3, 4], as well as the dependence upon stellar age and (bio)geochemical cycling [5, 6]. The definition of the Habitable Zone, that is the circumstellar region in which the global mean surface temperature of a planet permits the persistence of liquid water, initially enabled a binary view of whether a planet, as a whole, may be habitable [7, 8]. The increasing popularity of using climate models, including 2D energy balance models and 3D general circulation models (GCMs), to study exoplanetary climate has further introduced a variety of definitions for sub-planetary-scale surface habitability: temperature ranges optimal for complex or human life [e.g. 9–12], ice-free fraction [13–17], temperature ranges in which liquid water may persist [18–20], and finally of water availability through the consideration of water fluxes on land [21]. However, none of these definitions have yet been validated against how life is spatially distributed across Earth. With recent detections of potentially habitable exoplanets [e.g. 22, 23] and advances in the characterisation of rocky planet atmospheres [e.g. 24–28], it should therefore be a priority to consider how the use of GCMs can best assist the observational community in the search for potentially habitable planets. In this way, we aim to not only review a set of popular climatologically-based metrics of surface habitability with respect to modern Earth-based surface life but additionally define a new metric of surface habitability which better reflects the spatial patterns of life on Earth.

On Earth, life exists and thrives across a multitude of habitats with varying physicochemical conditions, including temperature, pH, pressure, salinity, and radiation exposure [3]. Upon the surface, complex multi-cellular life tends to dwell and thrive in the more temperate regions of Earth, whilst some life, particularly microbial, is able to thrive over a wider range of temperatures spanning from -20 to 122°C [3, 10, 29]. Common to all known lifeforms is a requirement for liquid water, as a solvent, along with sources of energy and nutrients [30]. Whilst necessary, the presence of liquid water alone is not sufficient to imply an abundance of life; with such an example seen in the oligotrophic gyres of the Earth’s oceans [31, 32]. Similarly, it is possible for life to exist in frozen conditions, for example, algal blooms observed within and underneath sea ice, the evolution of antifreeze proteins within fish, or microbes within cryoconite or brine pockets [33–37]. These examples not only highlight the extraordinary adaptive capabilities of life but also the importance of nutrients in considerations of habitability [30, 38]. The anisotropic distribution of nutrients across the Earth is, in part, determined by transport through atmospheric and hydrological dynamics (e.g. aeolian transport and ocean upwelling), as well as surface processes such as chemical weathering and outgassing [6, 39–41]. In this way, spatial patterns of surface habitability

may be tied to the atmospheric dynamics, which in turn are determined by properties including planetary rotation rate, insolation, and atmospheric composition [42–45].

Many studies of extraterrestrial surface habitability apply a binary assignment of habitable or uninhabitable, yet their definitions are based upon assumptions which do not completely consider the factors discussed above [e.g. 15, 18, 19]. Although life is indeed less prevalent in more extreme environments, it is important to consider that the greatest contributor to Earth’s main current biosignature, atmospheric oxygen, is plausibly attributable to photosynthetic bacteria during the Great Oxygenation Event [46]. Furthermore, microbial life has not only dominated for the majority of Earth’s biological history, but is also responsible for approximately half of global primary production, that is, the fixation of carbon into organic material through photosynthesis [46, 47]. On the other hand, human life has also had a significant impact upon the Earth’s climate, both modifying Earth’s atmospheric composition along with the production of potentially detectable technosignatures [48–50]. Investigations of surface habitability should therefore include the range of climatological conditions within which both microbial and complex life can flourish, and in particular, to the extent such that its existence may be detectable [51].

Putting these considerations together, we propose a novel climatologically-based metric of surface habitability, which explicitly considers the temperature ranges required by current, known life, as well as establishing a requirement for water availability through the consideration of surface water fluxes. Furthermore, nutrient availability is implicitly considered within the definition through the atmospheric-driven processes of transport and weathering which are linked to the water availability condition. Applied to geospatial data, the metric allows an examination into the spatial patterns of surface habitability as well as being reduced into a global habitable fraction. This offers the opportunity to examine instantaneous snapshots of planetary climate and investigate how patterns and fractional habitability may develop and change over geological timescales on a single planet, as well as providing a framework for inter-comparisons of habitability across model or planetary configurations [e.g. 52–56]. Furthermore, the metric distinguishes between areas which harbour climatological conditions more suitable for either microbial or macroscopic complex life as we see on Earth. Future applications of the metric may consider the generation of detectable biosignatures and/or technosignatures, for example through the coupling with or forcing of models which explore the biosphere-climate interaction [51, 57, 58]. In tandem with using Earth as a test-bed for the metric, this also leads to the potential of exploring *superhabitable* conditions, in which a planet may be considered to be more habitable than Earth, for example through a higher habitable fraction [59].

The new metric of surface habitability will be defined in Section 4.1, followed by an outline of the data and methods in Section 4. A selection of surface habitability metrics, including our newly defined metric, are then validated against the distribution of photosynthetic life on Earth in Section 2. Concluding remarks are given in Section 5.

2 Results and discussion

The broad spatial pattern of observed surface habitability shows *complex* habitability around the equator and mid-latitudes, with *microbial* and eventually *limited* habitability assigned at higher latitudes and altitudes (Fig. 1a). Upon land, *complex* habitability also extends into the sub-tropical latitudes, with the exception of the Sahara desert and Himalaya. In comparison with the mean surface climate, habitability at lower latitudes seems to be limited by areas of negative net precipitation ($P - E$), higher latitudes limited by colder temperatures and resultant presence of ice, and *microbial* marine habitability coincides with the Marginal Ice Zone (Fig. A1).

Comparing the observed habitability to the habitability metrics based purely on surface air temperature (T_s), it is immediately apparent that the spatial pattern of habitability is not fully captured (Fig. 1a, c-e). In particular, although the high latitudes are correctly labelled as *limited* habitability, lower latitude areas such as the Sahara and marine oligotrophic gyres have been incorrectly labelled as habitable. In the terrestrial domain, the validation statistics for these metrics indicate a statistically significant relationship with observed habitability and moderate metric performance with PC ranging from 0.68-0.75 and HSS 0.33-0.40 (Table 1). Although still statistically significant, the temperature-based metrics show little predictive skill in the marine domain with HSS of -0.03-0.06 and PC 0.37-0.52, likely due to the incorrect categorisation of the subtropical gyres. The lower performance in the marine domain also impacts the global results, where H^{S08} shows a higher PC but lower HSS than H^{S16} and H^{S19} . The validation results of H^{S16} and H^{S19} are remarkably similar despite the slight difference in habitability criteria, namely a 20K and 5K difference respectively in the upper and lower limit of *complex* habitability as well as the use of biotemperature (T_{bio}) within the H^{S19} definition (Table 1). Whilst H^{S19} shows slightly improved performance, the improvement is perhaps not as high as to be expected given that the definition being specifically based upon the temperature range optimal for terrestrial plant photosynthesis [12]. The H^{IF} metric, which is defined using sea ice concentration (SIC), shows a similar issue of not being able to capture the low-latitude areas of *limited* habitability in addition to the limitation of only being applicable to the marine domain. The H^{IF} validation results are also unsurprisingly similar to the H^{S08} marine values, given the close relationship between the presence of sea ice and T_s [60].

The metrics defined by aridity index (AI), H^{DG19H} and H^{DG19NA} , are limited to the terrestrial domain through the definition of AI making use of potential evapotranspiration (PET ; Eqn. 4). Qualitatively, these metrics seem to better capture some of the areas of *limited* habitability seen at higher altitudes (including the Andes, Himalaya, and the Rockies) and more arid regions (including the Sahara and the Great Australian Desert; Fig. 1g,h). However, both metrics respectively over- and underestimate the extent of *limited* habitability in these regions, as well as incorrectly assign the Greenland and Antarctic ice sheets as habitable. The validation statistics indicate better performance from H^{DG19NA} with a PC of 0.70 and HSS 0.15, whilst H^{DG19H} shows little predictive skill with HSS of -0.04 (Table 1). Aside from the metric accuracy of H^{S16} , the temperature-based metrics outperform both AI -based metrics in the terrestrial domain in all other respects, as well as being applicable to the marine

Table 1 Validation statistics and global habitable fraction for each metric and domain against the *observed* habitability. Optimal metric values have been highlighted in bold. The observed fractional habitability for each domain is listed in bold in the row of each respective domain label. PC represents proportion correct (or equivalently, metric accuracy), HSS Heidke Skill Score, f_H fractional habitability. Unless otherwise stated, χ^2 scores have $p=0.0000$ with 1 degree of freedom.

Domain & Metric	Microbial				Complex			
	PC	HSS	χ^2	f_H	PC	HSS	χ^2	f_H
Global				0.59				0.36
H^{W24}	0.67	0.34	4906	0.53	0.70	0.36	5455	0.41
H^{S08}	0.59	0.05	135	0.85	-	-	-	-
H^{S16}	-	-	-	-	0.46	0.10	1333	0.85
H^{S19}	-	-	-	-	0.47	0.10	990	0.82
Marine				0.55				0.29
H^{W24}	0.64	0.28	2250	0.49	0.66	0.25	1898	0.40
H^{S08}	0.52	-0.03	83	0.89	-	-	-	-
H^{S16}	-	-	-	-	0.38	0.06	671	0.89
H^{S19}	-	-	-	-	0.37	0.02	31	0.84
H^{IF}	0.53	-0.02	31	0.90	-	-	-	-
Terrestrial				0.71				0.53
H^{W24}	0.77	0.48	2881	0.62	0.80	0.60	4287	0.45
H^{S08}	0.75	0.36	1566	0.75	-	-	-	-
H^{S16}	-	-	-	-	0.68	0.33	1615	0.75
H^{S19}	-	-	-	-	0.71	0.40	2523	0.78
H^{DG19H}	0.52	-0.04	22	0.60	-	-	-	-
H^{DG19NA}	0.70	0.15	326	0.85	-	-	-	-

domain. To summarise, the metrics discussed so far are able to partially, but importantly not completely, describe the patterns of surface habitability seen on Earth. Furthermore, the patterns described by metrics dependent on T_s are different to those dependent upon AI , and it may therefore be concluded that a metric definition should incorporate both elements in order to describe more wholly the patterns of surface habitability on Earth. Furthermore, it would be beneficial to replace the use of AI with some alternate condition that not only improves upon the patterns of habitability captured in the terrestrial domain, but also is able to additionally capture the lower latitude *limited* habitability in the marine domain.

Reviewing the validation results of our metric, H^{W24} , we find an overall improved performance relative to the other metrics across all domains for both *microbial* and *complex* habitability (Table 1). Qualitatively, H^{W24} better captures the patterns of observed surface habitability, which is also reflected in the higher accuracies of 0.67 for *microbial* and 0.70 respectively for *complex* habitability, which with higher HSS (0.34 and 0.36, respectively) may be attributed to an improved predicted skill (Fig. 1). The metric performs particularly well in the terrestrial domain, with PC and HSS of 0.80 and 0.60 for *complex* habitability, and 0.77 and 0.48 for *microbial*. Large regions of *limited* habitability, including the Himalaya, Sahara, Greenland and Antarctica are all correctly predicted by the metric (Fig. 1). There is some disagreement between H^{W24} and the observed in the latitude at which habitability shifts from *complex* to

microbial, particularly on the Eurasian continent north of the Himalaya. The reduced habitability of the mountain ranges is somewhat captured by the metric, although with some differences to the observed at a finer scale; for example, there is some disagreement in the spatial pattern of habitability across the Andes, and although the spatial patterns are similar in the Rockies, the metric has under-predicted the habitability category. Australia in particular is not well captured, with H^{W24} generally indicating *limited* habitability with the observed showing *microbial* habitability across the Great Australian Desert with *complex* along the north-east coastlines.

These differences in the terrestrial domain may be attributed to the assumptions made by the metric. Firstly, whilst an annual mean climate was used to as an input for simplicity and transferability to other planetary configurations including tidally-locked climates, its use ignores the seasonal nature of life on Earth. In particular, the assignment of *microbial* habitability in the northern latitudes on the Eurasian continent results from an annual mean T_s between 253.15K and 273.15K. Although it holds that the northern temperate and boreal forest are unproductive during winter due to the suppression of photosynthesis at sub-zero temperatures, they are highly productive in the summer when no longer limited by temperatures resulting in the long term accumulation of biomass [61, 62]. Secondly, the metric is limited to considering only P and E within its water availability condition, which although is sufficient in representing the local atmospheric water balance, excludes many other terrestrial processes which are non-negligible in the global water cycle as well as being subject to human influence; such examples include surface runoff and fluvial transport, glacial outflow, snow-melt, and groundwater flow [63, 64]. Whilst we focus here upon the atmospheric influence on surface water fluxes and highlight the simplicity in using solely P and E , future work may wish to incorporate these other factors within future definitions of habitability, and investigate whether this improves the habitability categorisation of the water-limited regions such as the mountain ranges and Australia. However, within the context of exoplanet habitability and current observational capabilities, this level of granularity may not be necessary given that our metric is able to capture the broad-scale patterns of habitability [65].

Although the metric is less accurate in the marine domain (0.64 and 0.66 respectively for *microbial* and *complex* habitability) than on land, the higher HSS values indicate a vast improvement in predictive skill in comparison to the other metrics (Table 1). Qualitatively, the latitudinal shift from *complex* to *microbial* habitability as well as the *limited* habitability of sub-tropical gyres are well-captured (Fig. A1). There is also some disagreement in the habitability of the high Arctic, which the metric predicts as *microbial* whilst the observed almost directly shifts from *complex* to *limited*. However, in addition to the previously discussed low sun angle limitations of the OC-CCI Chl a dataset, satellite-derived datasets of Chl a are also susceptible to pixel contamination introduced by nearby sea ice or mixed ice/ocean pixels and additionally show difficulty in detecting under ice blooms [66, 67]. In this way, it may be that OC-CCI Chl a underestimates the true abundance of phytoplankton in the presence of sea ice, and accordingly the resultant observed habitability categorisation. Another disagreement lies across the Indian and Western Pacific oceans, whereby the metric predicts large-scale *complex* habitability whilst the Arabian Sea which is assigned as

limited. However, the observed shows the inverse, with the Indo-Pacific Warm Pool typically showing low levels of productivity due to nutrient limitation, whilst the monsoonal winds in the Arabian sea contribute towards a vertical mixing which, along with aeolian transport of iron fluxes, refreshes nutrient stocks and subsequently increases productivity [68–70]. Similarly, the higher habitability observed particularly along the western coast shorelines, which can be attributed to enhanced nutrient availability, has not been captured by our metric [71, 72]. In this way, the $P - E$ condition in our metric is able to only partially capture the distribution of nutrients across the marine domain, and future work may aim to investigate using additional or alternate climate parameters to improve the metric accuracy.

Finally, comparing the fractional habitabilities f_H produced by the metrics finds that the temperature-based metrics all overestimate f_H in comparison to the observed across all domains (Table 1). The AI -based metrics straddle the observed terrestrial *microbial* f_H , with the same pattern of under/overestimation respectively seen in H^{DG19H} and H^{DG19NA} . Overall, H^{W24} shows f_H closest to the observed, with the exception of H^{S08} in the terrestrial domain for *microbial* habitability which is marginally closer to the observed f_H . However, the higher PC and HSS in H^{W24} indicates an overall more accurate and skillful representation of terrestrial *microbial* habitability than H^{S08} (Table 1).

3 Figures

4 Methods

4.1 Metric description

Our habitability metric is defined using three climatological variables: surface air temperature T_s [K], precipitation P [$\text{mm year}^{-1}_{\oplus}$], and evaporation E [$\text{mm year}^{-1}_{\oplus}$]. Temperature was chosen over variables which directly relate to radiation, such as UV flux or photosynthetically active radiation (PAR), in order to focus upon the surface climate itself as well as to not discriminate toward pigments (such as Chlorophyll- a) or biochemical reactions optimal to the solar spectral energy distribution [73]. Firstly, two temperature ranges are defined, representing the thermal limits for *microbial* and *complex* life, respectively. The microbial range is based upon the observed limits of extremophilic microbial life [3, 74, 75], whilst the complex life range is a conservative estimate in which the majority of multicellular poikilotherms are known to inhabit, as defined by [10]:

$$H_T(T_s) = \begin{cases} \text{complex} & \text{if } 273.15 \leq T_s \leq 323.15 \text{ K,} \\ \text{microbial} & \text{if } 253.15 \leq T_s \leq 395.15 \text{ K,} \\ \text{limited} & \text{otherwise.} \end{cases} \quad (1)$$

Although the microbial temperature range in Eqn. (1) includes water outside of the liquid state at 1 bar pressure, retaining this range acknowledges both the fully observed limits of life whilst also allowing investigations into other environments, for

example different atmospheric pressures or salinity, in which water may still exist in liquid form outside of 0-100°C. The second condition for habitability is based upon the requirement for liquid water [30], which we extend to a general condition of water availability through the consideration of surface water fluxes as represented by precipitation P minus evaporation E , along with a minimum precipitation rate equivalent to the definition of a desert on Earth [76]:

$$H(T_s, P, E) = \begin{cases} H_T(T_s) & \text{if } P - E \geq 0 \text{ \& } P \geq 250 \text{ mm year}^{-1}, \\ \text{limited} & \text{otherwise.} \end{cases} \quad (2)$$

Whilst the concept of water availability is not new to terrestrial investigations of primary productivity [62], it may at first seem an unusual condition to apply to the oceans which are obviously abundant in water. However, we highlight here that patterns of P and E are influenced by atmospheric dynamics and as such are related to other variables such as surface wind which influence the transport and subsequent availability of nutrients [39, 40]. Put together, Eqn. 2 is a binary requirement for a habitable environment, whilst Eqn. 1 controls the assignment of *microbial* versus *complex* habitability. If either Eqn. 1 or Eqn. 2 is not satisfied, then the habitability category is assigned as *limited*. We emphasise that these categories are non-strict in the sense that they provide an indication of the predominant form (or absence) of life, so for example, it is possible that *complex* life may inhabit areas designated as *microbial* or *limited* habitability. Additionally, it is important to note that *complex* habitability is a subset of *microbial* habitability, thus, an environment marked as *complex* habitability should likely be inhabited by both complex and microbial life. For studies of hypothetical habitability on water-limited worlds [e.g. 9, 77], we suggest only applying the temperature limits (Eqn. 1).

4.2 Data

4.2.1 Earth climatological data

All metrics make use of the ERA5 global monthly reanalysis [78] to calculate the 2D surface habitability of Earth. In particular, the variables used amongst the habitability metrics include surface air temperature (T_s), evaporation (E), potential evapotranspiration (PET), precipitation (P), and sea ice concentration (SIC). ERA5 lies on a $0.25^\circ \times 0.25^\circ$ latitude-longitude grid and although shows some bias in precipitation over the tropics is considered to perform well in representing global surface climate in comparison to observation and other reanalyses [78–80].

4.2.2 Earth observed habitability data

Photosynthetic life was chosen as an analogue for the abundance and distribution of life on Earth for two main reasons: firstly, photosynthetic life dominates the biomass on terrestrial Earth, with plants contributing up to ~80% and bacteria ~15% of Earth’s terrestrial biomass [81]. Although primary producers only account for 20% of Earth’s marine biomass, they remain the main contributor in sustaining higher trophic levels

[47, 82]. Secondly, the pigment Chlorophyll-*a*, used by most photosynthetic life, produces a unique reflectance spectrum in which remote sensing techniques are able to generate global-scale datasets which are representative of biomass.

Since there is no single global dataset of photosynthetic life, the monthly MODIS Terra data product of Normalised Difference Vegetation Index [NDVI; 83] and OC-CCI v6.0 data product of monthly mean surface Chlorophyll-*a* concentration [Chl *a*; 84] were selected to represent terrestrial and marine life, respectively. MODIS NDVI lies on a 9km latitude-longitude grid and represents vegetation density and health through the measurement of the difference ratio in spectral reflectance between the visible red and near-infrared regions. OC-CCI Chl *a* is an ocean colour product representing the abundance of phytoplankton through the measurement of the ratio of blue to green light that is reflected. It lies on a 4km latitude-longitude grid and is an aggregate of data from multiple satellites which is validated against in-situ data [84]. Due to the high viewing angle and presence of sea ice, the product lacks data for latitudes exceeding 50° during the respective hemispheric winter months. To circumvent this issue, the Chl *a* monthly climatology was linearly interpolated across the months with missing data, and the resulting interpolated values weighted by the respective sea ice concentration sourced from the HadISST reanalysis [85, 86]. A minimum value of Chl *a* was set to 0.01 mg m⁻³, in line with observed under-ice values [87, 88]. The HadISST dataset incorporates both satellite and in-situ data which is then interpolated to provide spatially continuous monthly data at a 1°×1° resolution on a latitude-longitude grid.

These remotely sensed variables were chosen so as to avoid any further introduction of bias from modelled variables such as primary productivity or biomass, whilst retaining a strong correlation to the density and distribution of photosynthetic life [89, 90]. With this in mind, both products are susceptible to some bias, mostly at higher values where the signal becomes saturated [e.g. 91, 92], although not problematic for our validation which sets thresholds for *microbial* and *complex* habitability at low to intermediate values of NDVI and Chl *a*. In addition to the seasonal high-latitude data gaps discussed above, OC-CCI Chl *a* additionally shows a positive bias for values less than 0.3 mg m⁻³ which increases in magnitude with decreasing Chl *a*¹.

4.3 Methods

4.3.1 Data pre-processing and metric habitability

Each dataset (ERA5, NDVI, and OC-CCI Chl *a*) was regridded to a 1°×1° latitude-longitude grid, to match the dataset with the coarsest resolution, HadISST SIC. Land and sea masks were applied to the terrestrial (NDVI) and marine (OC-CCI Chl *a*) observational data, respectively. Monthly mean climatologies across 2003-2018 were first calculated, with the year range selected for maximum temporal overlap across datasets, as well as over a long enough period to reduce the influence on climate from inter-annual climate variability. At this stage, the gap-filling for OC-CCI Chl *a* was performed, as well as the calculations of biotemperature T_{bio} and aridity index AI which are used in the [12] and [21] metrics, respectively. T_{bio} represents the optimal

¹Source: [OC-CCI Ocean Color Product User Guide for v6.0](#)

Table 2 Overview of metrics used in the comparison of surface habitability on Earth with the conditions required for *complex* and *microbial* habitability categories and the domain over which each metric is valid. T_s represents surface air temperature, T_{bio} biotemperature, SIC sea ice concentration, AI aridity index.

Metric [Reference]	Microbial	Complex	Domain
H^{W24} [this work]	Eqns. 1 & 2		Global
H^{S08} [18, 19]	$273.15 \leq T_s \leq 373.15$ K	n/a	Global
H^{S16} [10]	n/a	$273.15 \leq T_s \leq 323.15$ K	Global
H^{S19} [12]	n/a	$277.65 < T_{\text{bio}} < 303.15$ K	Global
H^{IF} [15]	$SIC < 0.15$	n/a	Marine
H^{DG19H} [21]	$AI > 0.39$	n/a	Terrestrial
H^{DG19NA} [21]	$AI \geq 0.17$	n/a	Terrestrial

range for the occurrence of terrestrial photosynthesis and is defined as:

$$T_{\text{bio}} = \begin{cases} 303.15 & \text{if } T_s \geq 303.15\text{K}, \\ 273.15 & \text{if } T_s \leq 273.15\text{K}, \\ T_s & \text{otherwise,} \end{cases} \quad (3)$$

for surface air temperature T_s [12]. The aridity index AI is defined as:

$$AI = \frac{P}{P + PET}, \quad (4)$$

for precipitation P and potential evapotranspiration PET , where lower values of represent a more arid environment [21]. Finally, an annual mean climate across this period was calculated for all variables from the monthly climatologies. The 2D surface habitability was calculated for each metric outlined in Table 2, noting that the H^{S16} metric takes inspiration from the climate classifications of [12] and explores a definition specific to photosynthetic life. For each of the *microbial* and *complex* categories, the resultant fractional habitability f_H was calculated as the weighted fraction of all grid cells which satisfy the respective habitability conditions, following [18]. To aid comparison, where previous metric definitions have relied upon a binary assignment of habitability, unless otherwise specified by the study, a *habitable* assignment is here relabeled as *microbial*. In addition to examining global habitability where possible, we also examine the habitability of marine and terrestrial domains individually, enabling a comparison of metrics only applicable to either of these domains.

4.3.2 Observed habitability calculation

The global *observed* habitability H^{obs} was calculated as the sum of the *observed* terrestrial and marine habitability, H_T^{obs} and H_M^{obs} respectively, which were in turn defined through the application of threshold values to annual mean NDVI ($\text{NDVI}_{\text{mean}}$) and

Chl a (Chl a_{mean}), and additionally the annual minimum Chl a (Chl a_{min}):

$$H_T^{\text{obs}} = \begin{cases} \text{complex} & \text{if } \text{NDVI}_{\text{mean}} > 0.3, \\ \text{microbial} & \text{if } \text{NDVI}_{\text{mean}} > 0.15, \\ \text{limited} & \text{otherwise,} \end{cases} \quad (5)$$

$$H_M^{\text{obs}} = \begin{cases} \text{complex} & \text{if } \text{Chl } a_{\text{min}} > 0.15 \text{ mg m}^{-3}, \\ \text{microbial} & \text{if } \text{Chl } a_{\text{mean}} > 0.15 \text{ mg m}^{-3}, \\ \text{limited} & \text{otherwise.} \end{cases} \quad (6)$$

The *microbial* habitable threshold of the terrestrial (NDVI) data is taken at the maximum limit of the NDVI of bare ground, soil, sand, and rock, which typically show values of 0–0.15 [93–95]. The threshold of 0.3 for terrestrial *complex* habitability is based on the average annual mean NDVI of all biomes excluding bare ground as described in [96], as well as being the green threshold used in the sample MODIS NDVI figure².

The marine *complex* and *microbial* thresholds are defined as where the annual minimum and mean Chl a exceeds 0.15 mg m^{-3} , respectively. Although marine trophic states are commonly used to categorise the marine environment, definitions are often subjective and vary between ecosystem with ranges of $0.07\text{--}0.1 \text{ mg m}^{-3}$ often cited as the crossover from oligotrophic to mesotrophic environments in the open ocean despite surface Chl a in known oligotrophic environments seasonally exceeding this range [32, 97–101]. Acknowledging the slight positive bias seen in lower values in the OC-CCI Chl a dataset (Section 4.2), a slightly higher threshold value of 0.15 mg m^{-3} was selected, which corresponds to a shift from abundance in picoplankton to nano- and microplankton as well as from phytoplankton to mesozooplankton [102, 103]. The use of both annual minimum and mean Chl a values acknowledges the short turnover time ($\sim 2\text{--}6$ days) of phytoplankton: where the annual minimum exceeds the threshold implies the ability to continually support higher trophic states (i.e. complex life) year-round, whilst the use of an annual mean recognises the seasonal abundance of phytoplankton [i.e. microbial life; 47, 104]. It is important to note here that the turnover time for terrestrial primary producers is around 19 years, hence why it is sufficient to use only annual mean values for the NDVI threshold [47]. Although there exist other datasets representative of macroscopic life such as the biodiversity or species richness of marine mammals, these generally rely upon empirical observation which are subject to data quality issues including spatiotemporal biases, gaps, and errors, as well as differences in data collection methodology [105, 106]. In any case, the use of an annual minimum and mean Chl a appears qualitatively well-constrained with the declining abundance of higher trophic levels at the higher latitudes [107, 108].

4.3.3 Metric validation

Each habitability metric was compared to the *observed* habitability by means of a qualitative spatial comparison, as well as quantitatively through computation of the

²Source: MODIS/Terra Vegetation Indices Monthly L3 Global 0.05Deg CMG V061

chi-squared “test of independence” statistic (χ^2), proportion correct or equivalently metric accuracy (PC), and the Heidke Skill Score [HSS; 109]. Computation of accuracy and skill scores is common to forecast verification in weather prediction [109–113], but has also been applied to GCMs [114–116] and remote sensing algorithms and datasets [117, 118]. In particular, HSS measures the predictive power of the forecast relative to random chance, where a score of 0 implies that the forecast performs no better than random chance and a score of 1 implies a perfect forecast [109].

For each metric, relevant habitability category (*microbial* and/or *complex*) and domain (global, terrestrial, and/or marine), a contingency table of metric-generated “predicted” and observed habitability was created, from which these three statistics were computed. The contribution of each grid cell to the contingency table was weighted with respect to its area, such that the smaller grid cells towards the high latitudes receive a lower weight than those towards the equator. The combination of statistics allows for a more robust validation of each metric, whereby the proportion correct represents the metric accuracy, HSS attributes the accuracy to skill versus random chance, and χ^2 the statistical significance of the predicted and observed habitability belonging to the same population.

5 Conclusion

We have reviewed a set of climate-based metrics of surface habitability against the distribution of photosynthetic life on Earth, finding that a metric defined using either surface air temperature T_s , aridity index AI , or sea ice concentration SIC alone is not sufficient in capturing the pattern of habitability on Earth. Metrics dependent upon T_s and SIC approximately capture the shift to *microbial* and *limited* habitability at higher latitudes, but incorrectly label regions of observed *limited* habitability regions at lower latitudes as habitable, resulting in an overestimation in the fractional habitability f_H . The metrics dependent upon AI show different patterns of habitability to T_s which begin to resemble some of the lower latitude terrestrial regions of *limited* habitability but exhibit poor predictive skill overall. We find that our newly defined metric, defined using T_s , precipitation P , and evaporation E , shows a vast improvement to the other metrics, with the highest accuracy, predictive skill, and (mostly) closest f_H to the observed. Globally, our metric has accuracies of 0.67 and 0.70 for *microbial* and *complex* habitability respectively, and performs particularly well in the terrestrial domain with respective accuracies of 0.77 and 0.80. Disagreements between our metric and the observed can be attributed to a mixture of uncertainties from the data sources used to calculate observed habitability, seasonal variability, as well as the metric failing to entirely capture the distribution of nutrients across the marine domain. The incorporation of additional climate parameters may serve to better describe the global distribution of nutrients as well as surface water fluxes, however we leave this for future work to investigate, noting the simplicity of the metric in its current form. Finally, we highlight that use of our metric considers that other requirements of habitability, including active carbon cycle and plate tectonics, suitable atmospheric composition, and spectral energy distribution, as satisfied [7, 30]. In this

way, we suggest that the metric be used in tandem with other measures of habitability, including but not limited to, carbon cycle models, Habitable Zone and Habitable Zone Lifetimes, Gaia modelling, or nutrient availability [5, 119–121].

Supplementary information.

Acknowledgements. The authors thank Ian Crawford for providing constructive feedback on preliminary drafts of this work. H.L.W. acknowledges support from NERC via the London NERC DTP [Grant NE/S007229/1]. N.J.M. acknowledges support from a UKRI Future Leaders Fellowship [Grant MR/T040866/1], a Science and Technology Facilities Funding Council Nucleus Award [Grant ST/T000082/1], and the Leverhulme Trust through a research project grant [RPG-2020-82].

Data availability

The ERA5 monthly dataset [78] is available for download from the [123]. MODIS Terra NDVI [MOD13C2 v061; 83] is available for download at doi.org/10.5067/MODIS/MOD13C2.061. The OC-CCI monthly Chlorophyll-*a* ocean colour dataset [v6.0; 84] is available for download at oceancolor.org. HadISST monthly sea ice concentration [85, 86] is available for download at metoffice.gov.uk/hadobs/hadisst.

Code availability

The project codebase is available at github.com/hannahwoodward/2024-hab-metrics.

Appendix A Extended Data

References

- [1] Gonzalez, G. The galactic habitable zone: Galactic chemical evolution. *Icarus* **152**, 185–200 (2001). URL <http://dx.doi.org/10.1006/icar.2001.6617>.
- [2] Lineweaver, C. H., Fenner, Y. & Gibson, B. K. The galactic habitable zone and the age distribution of complex life in the milky way. *Science* **303**, 59–62 (2004). URL <https://doi.org/10.1126/science.1092322>.
- [3] Merino, N. *et al.* Living at the extremes: Extremophiles and the limits of life in a planetary context. *Frontiers in Microbiology* **10** (2019). URL <http://dx.doi.org/10.3389/fmicb.2019.00780>.
- [4] Ratliff, L. *et al.* The vacant niche revisited: Using negative results to refine the limits of habitability. *preprint* (2023). URL <http://dx.doi.org/10.1101/2023.11.06.565904>.

- [5] Rushby, A. J., Claire, M. W., Osborn, H. & Watson, A. J. Habitable zone lifetimes of exoplanets around main sequence stars. *Astrobiology* **13**, 833–849 (2013). URL <http://dx.doi.org/10.1089/ast.2012.0938>.
- [6] Rushby, A. J., Johnson, M., Mills, B. J., Watson, A. J. & Claire, M. W. Long-term planetary habitability and the carbonate-silicate cycle. *Astrobiology* **18**, 469–480 (2018). URL <https://doi.org/10.1089%2Fast.2017.1693>.
- [7] Kasting, J. F., Whitmire, D. P. & Reynolds, R. T. Habitable zones around main sequence stars. *Icarus* **101**, 108–128 (1993). URL <http://dx.doi.org/10.1006/icar.1993.1010>.
- [8] Kopparapu, R. K. *et al.* Habitable zones around main-sequence stars: New estimates. *The Astrophysical Journal* **765**, 131 (2013). URL <http://dx.doi.org/10.1088/0004-637x/765/2/131>.
- [9] Lobo, A. H., Shields, A. L., Palubski, I. Z. & Wolf, E. Terminator habitability: The case for limited water availability on m-dwarf planets. *The Astrophysical Journal* **945**, 161 (2023). URL <http://dx.doi.org/10.3847/1538-4357/aca970>.
- [10] Silva, L., Vladilo, G., Schulte, P. M., Murante, G. & Provenzale, A. From climate models to planetary habitability: temperature constraints for complex life. *International Journal of Astrobiology* **16**, 244–265 (2016). URL <http://dx.doi.org/10.1017/s1473550416000215>.
- [11] Silva, L., Vladilo, G., Murante, G. & Provenzale, A. Quantitative estimates of the surface habitability of kepler-452b. *Monthly Notices of the Royal Astronomical Society* **470**, 2270–2282 (2017). URL <https://doi.org/10.1093/mnras/stx1396>.
- [12] Stevenson, D. S. Phytoclimatic mapping of exoplanets. *International Journal of Astrobiology* **19**, 68–77 (2019). URL <https://www.cambridge.org/core/product/68C46D4C29719FC6E7602B60DCD561FF>.
- [13] Genio, A. D. D. *et al.* Habitable climate scenarios for proxima centauri b with a dynamic ocean. *Astrobiology* **19**, 99–125 (2019). URL <https://doi.org/10.1089%2Fast.2017.1760>.
- [14] Hu, Y. & Yang, J. Role of ocean heat transport in climates of tidally locked exoplanets around m dwarf stars. *Proceedings of the National Academy of Sciences* **111**, 629–634 (2013). URL <https://doi.org/10.1073%2Fpnas.1315215111>.
- [15] Sergeev, D. E. *et al.* The trappist-1 habitable atmosphere intercomparison (thai). ii. moist cases—the two waterworlds. *The Planetary Science Journal* **3**, 212 (2022). URL <http://dx.doi.org/10.3847/psj/ac6cf2>.

- [16] Turbet, M. *et al.* The habitability of Proxima Centauri b. *A&A* **596**, A112 (2016). URL <https://doi.org/10.1051/0004-6361/201629577>.
- [17] Yang, J., Ji, W. & Zeng, Y. Transition from eyeball to snowball driven by sea-ice drift on tidally locked terrestrial planets. *Nature Astronomy* **4**, 58–66 (2020). URL <https://doi.org/10.1038/s41550-019-0883-z>.
- [18] Jansen, T., Scharf, C., Way, M. & Del Genio, A. Climates of warm earth-like planets. ii. rotational “goldilocks” zones for fractional habitability and silicate weathering. *The Astrophysical Journal* **875**, 79 (2019). URL <https://dx.doi.org/10.3847/1538-4357/ab113d>.
- [19] Spiegel, D. S., Menou, K. & Scharf, C. A. Habitable climates. *The Astrophysical Journal* **681**, 1609 (2008). URL <https://dx.doi.org/10.1086/588089>.
- [20] Vladilo, G. *et al.* The habitable zone of earth-like planets with different levels of atmospheric pressure. *The Astrophysical Journal* **767**, 65 (2013). URL <https://dx.doi.org/10.1088/0004-637X/767/1/65>.
- [21] Del Genio, A. D. *et al.* Climates of warm earth-like planets. iii. fractional habitability from a water cycle perspective. *The Astrophysical Journal* **887**, 197 (2019). URL <https://dx.doi.org/10.3847/1538-4357/ab57fd>.
- [22] Luger, R. *et al.* A seven-planet resonant chain in trappist-1. *Nature Astronomy* **1** (2017). URL <http://dx.doi.org/10.1038/s41550-017-0129>.
- [23] Kossakowski, D. *et al.* The carmenes search for exoplanets around m dwarfs: Wolf 1069 b: Earth-mass planet in the habitable zone of a nearby, very low-mass star. *Astronomy & Astrophysics* **670**, A84 (2023). URL <http://dx.doi.org/10.1051/0004-6361/202245322>.
- [24] Claringbold, A. B., Rimmer, P. B., Rugheimer, S. & Shorttle, O. Prebiosignature molecules can be detected in temperate exoplanet atmospheres with jwst. *The Astronomical Journal* **166**, 39 (2023). URL <http://dx.doi.org/10.3847/1538-3881/acdacc>.
- [25] Lincowski, A. P. *et al.* Potential atmospheric compositions of trappist-1 c constrained by jwst/miri observations at 15 μ m. *The Astrophysical Journal Letters* **955**, L7 (2023). URL <http://dx.doi.org/10.3847/2041-8213/acee02>.
- [26] Moran, S. E. *et al.* High tide or riptide on the cosmic shoreline? a water-rich atmosphere or stellar contamination for the warm super-earth gj 486b from jwst observations. *The Astrophysical Journal Letters* **948**, L11 (2023). URL <http://dx.doi.org/10.3847/2041-8213/accb9c>.
- [27] Lustig-Yaeger, J. *et al.* A jwst transmission spectrum of the nearby earth-sized exoplanet lhs 475 b. *Nature Astronomy* (2023). URL <http://dx.doi.org/10.1038/>

s41550-023-02064-z.

- [28] Zieba, S. *et al.* No thick carbon dioxide atmosphere on the rocky exoplanet trappist-1c. *Nature* **620**, 746–749 (2023). URL <http://dx.doi.org/10.1038/s41586-023-06232-z>.
- [29] Anav, A. *et al.* Spatiotemporal patterns of terrestrial gross primary production: A review. *Reviews of Geophysics* **53**, 785–818 (2015). URL <http://dx.doi.org/10.1002/2015rg000483>.
- [30] Cockell, C. *et al.* Habitability: A review. *Astrobiology* **16**, 89–117 (2016). URL <http://dx.doi.org/10.1089/ast.2015.1295>.
- [31] Jones, E. G. & Lineweaver, C. H. To what extent does terrestrial life “follow the water”? *Astrobiology* **10**, 349–361 (2010). URL <https://doi.org/10.1089/ast.2009.0428>. Doi: 10.1089/ast.2009.0428.
- [32] McClain, C. R., Signorini, S. R. & Christian, J. R. Subtropical gyre variability observed by ocean-color satellites. *Deep Sea Research Part II: Topical Studies in Oceanography* **51**, 281–301 (2004). URL <http://dx.doi.org/10.1016/j.dsr2.2003.08.002>.
- [33] Ardyna, M. *et al.* Environmental drivers of under-ice phytoplankton bloom dynamics in the Arctic Ocean. *Elementa: Science of the Anthropocene* **8**, 30 (2020). URL <https://doi.org/10.1525/elementa.430>.
- [34] Clarke, A. *11 - Evolution and low temperatures*, 187–207 (Academic Press, London, 2003). URL <https://www.sciencedirect.com/science/article/pii/B9780125986557500380>.
- [35] Cook, J., Edwards, A., Takeuchi, N. & Irvine-Fynn, T. Cryoconite: the dark biological secret of the cryosphere. *Progress in Physical Geography: Earth and Environment* **40**, 66–111 (2016). URL <https://journals.sagepub.com/doi/abs/10.1177/0309133315616574>.
- [36] Fletcher, G. L., Hew, C. L. & Davies, P. L. Antifreeze proteins of teleost fishes. *Annual Review of Physiology* **63**, 359–390 (2001). URL <https://www.annualreviews.org/content/journals/10.1146/annurev.physiol.63.1.359>.
- [37] Price, P. B. Microbial life in glacial ice and implications for a cold origin of life. *FEMS Microbiology Ecology* **59**, 217–231 (2007). URL <https://doi.org/10.1111/j.1574-6941.2006.00234.x>.
- [38] Nicholson, A. E. *et al.* Predicting biosignatures for nutrient-limited biospheres. *Monthly Notices of the Royal Astronomical Society* **517**, 222–239 (2022). URL <https://doi.org/10.1093/mnras/stac2086>.

- [39] Pierrehumbert, R. T. The hydrologic cycle in deep-time climate problems. *Nature* **419**, 191–198 (2002). URL <https://doi.org/10.1038/nature01088>.
- [40] Walker, J. C. G., Hays, P. B. & Kasting, J. F. A negative feedback mechanism for the long-term stabilization of earth’s surface temperature. *Journal of Geophysical Research: Oceans* **86**, 9776–9782 (1981). URL <https://doi.org/10.1029/JC086iC10p09776>.
- [41] West, A. J., Galy, A. & Bickle, M. Tectonic and climatic controls on silicate weathering. *Earth and Planetary Science Letters* **235**, 211–228 (2005). URL <https://www.sciencedirect.com/science/article/pii/S0012821X05002116>.
- [42] Hammond, M. & Lewis, N. T. The rotational and divergent components of atmospheric circulation on tidally locked planets. *Proceedings of the National Academy of Sciences* **118** (2021). URL <https://doi.org/10.1073/pnas.2022705118>.
- [43] Haqq-Misra, J., Wolf, E. T., Joshi, M., Zhang, X. & Kopparapu, R. K. Demarcating circulation regimes of synchronously rotating terrestrial planets within the habitable zone. *The Astrophysical Journal* **852**, 67 (2018). URL <http://dx.doi.org/10.3847/1538-4357/aa9f1f>.
- [44] Kaspi, Y. & Showman, A. P. Atmospheric dynamics of terrestrial exoplanets over a wide range of orbital and atmospheric parameters. *The Astrophysical Journal* **804**, 60 (2015). URL <https://dx.doi.org/10.1088/0004-637X/804/1/60>.
- [45] Williams, D. A., Ji, X., Corlies, P. & Lora, J. M. Clouds and seasonality on terrestrial planets with varying rotation rates. *The Astrophysical Journal* **963**, 36 (2024). URL <https://dx.doi.org/10.3847/1538-4357/ad192f>.
- [46] Crockford, P. W., Bar On, Y. M., Ward, L. M., Milo, R. & Halevy, I. The geologic history of primary productivity. *Current Biology* **33**, 4741–4750.e5 (2023). URL <https://www.sciencedirect.com/science/article/pii/S0960982223012861>.
- [47] Field, C. B., Behrenfeld, M. J., Randerson, J. T. & Falkowski, P. Primary production of the biosphere: Integrating terrestrial and oceanic components. *Science* **281**, 237–240 (1998). URL <http://dx.doi.org/10.1126/science.281.5374.237>.
- [48] Haqq-Misra, J. *et al.* Detectability of chlorofluorocarbons in the atmospheres of habitable m-dwarf planets. *The Planetary Science Journal* **3**, 60 (2022). URL <https://dx.doi.org/10.3847/PSJ/ac5404>.
- [49] IPCC. *Summary for Policymakers* (Cambridge University Press, Cambridge, United Kingdom and New York, NY, USA, 2021).

- [50] Seager, S. *et al.* Fully fluorinated non-carbon compounds nf_3 and sf_6 as ideal technosignature gases. *Scientific Reports* **13**, 13576 (2023). URL <https://doi.org/10.1038/s41598-023-39972-z>.
- [51] Nicholson, A. E. & Mayne, N. J. A biotic habitable zone: impacts of adaptation in biotic temperature regulation. *Monthly Notices of the Royal Astronomical Society* **521**, 5139–5151 (2023). URL <https://doi.org/10.1093/mnras/stad848>.
- [52] Farnsworth, A. *et al.* Climate extremes likely to drive land mammal extinction during next supercontinent assembly. *Nature Geoscience* (2023). URL <https://doi.org/10.1038/s41561-023-01259-3>.
- [53] Fauchez, T. J. *et al.* Trappist-1 habitable atmosphere intercomparison (thai): motivations and protocol version 1.0. *Geoscientific Model Development* **13**, 707–716 (2020). URL <http://dx.doi.org/10.5194/gmd-13-707-2020>.
- [54] O'Malley-James, J. T., Cockell, C. S., Greaves, J. S. & Raven, J. A. Swansong biospheres ii: the final signs of life on terrestrial planets near the end of their habitable lifetimes. *International Journal of Astrobiology* **13**, 229–243 (2014). URL <https://www.cambridge.org/core/product/EC5E8031028203F2EA3866C170575922>.
- [55] Way, M. J., Davies, H. S., Duarte, J. C. & Green, J. A. M. The climates of earth's next supercontinent: Effects of tectonics, rotation rate, and insolation. *Geochemistry, Geophysics, Geosystems* **22**, e2021GC009983 (2021). URL <https://agupubs.onlinelibrary.wiley.com/doi/abs/10.1029/2021GC009983>.
- [56] Yang, J. *et al.* Simulations of water vapor and clouds on rapidly rotating and tidally locked planets: A 3d model intercomparison. *The Astrophysical Journal* **875**, 46 (2019). URL <https://dx.doi.org/10.3847/1538-4357/ab09f1>.
- [57] Arthur, R., Nicholson, A. E. & Mayne, N. J. What doesn't kill gaia makes her stronger (2024). URL <https://ui.adsabs.harvard.edu/abs/2024arXiv240505091A>. 12 pages, 7 figures.
- [58] Seager, S. Exoplanet habitability. *Science* **340**, 577–581 (2013). URL <https://doi.org/10.1126/science.1232226>.
- [59] Schulze-Makuch, D., Heller, R. & Guinan, E. In search for a planet better than earth: Top contenders for a superhabitable world. *Astrobiology* **20**, 1394–1404 (2020). URL <https://doi.org/10.1089/ast.2019.2161>.
- [60] Screen, J. A. & Simmonds, I. The central role of diminishing sea ice in recent arctic temperature amplification. *Nature* **464**, 1334–1337 (2010). URL <https://doi.org/10.1038/nature09051>.

- [61] Chen, M. *et al.* Regional contribution to variability and trends of global gross primary productivity. *Environmental Research Letters* **12**, 105005 (2017). URL <https://dx.doi.org/10.1088/1748-9326/aa8978>.
- [62] Nemani, R. R. *et al.* Climate-driven increases in global terrestrial net primary production from 1982 to 1999. *Science* **300**, 1560–1563 (2003). URL <https://doi.org/10.1126/science.1082750>.
- [63] Dai, A. & Trenberth, K. E. Estimates of freshwater discharge from continents: Latitudinal and seasonal variations. *Journal of Hydrometeorology* **3**, 660–687 (2002). URL https://journals.ametsoc.org/view/journals/hydr/3/6/1525-7541_2002_003_0660_eofdfc_2_0_co_2.xml.
- [64] Trenberth, K. E., Smith, L., Qian, T., Dai, A. & Fasullo, J. Estimates of the global water budget and its annual cycle using observational and model data. *Journal of Hydrometeorology* **8**, 758–769 (2007). URL https://journals.ametsoc.org/view/journals/hydr/8/4/jhm600_1.xml.
- [65] Fujii, Y. *et al.* Exoplanet biosignatures: Observational prospects. *Astrobiology* **18**, 739–778 (2018). URL <https://doi.org/10.1089/ast.2017.1733>.
- [66] Bélanger, S., Ehn, J. K. & Babin, M. Impact of sea ice on the retrieval of water-leaving reflectance, chlorophyll a concentration and inherent optical properties from satellite ocean color data. *Remote Sensing of Environment* **111**, 51–68 (2007). URL <https://www.sciencedirect.com/science/article/pii/S0034425707001289>.
- [67] Lowry, K. E., van Dijken, G. L. & Arrigo, K. R. Evidence of under-ice phytoplankton blooms in the chukchi sea from 1998 to 2012. *Deep Sea Research Part II: Topical Studies in Oceanography* **105**, 105–117 (2014). URL <https://www.sciencedirect.com/science/article/pii/S0967064514000782>.
- [68] Gao, Y., Kaufman, Y. J., Tanré, D., Kolber, D. & Falkowski, P. G. Seasonal distributions of aeolian iron fluxes to the global ocean. *Geophysical Research Letters* **28**, 29–32 (2001). URL <https://doi.org/10.1029/2000GL011926>.
- [69] Westberry, T. K., Silsbe, G. M. & Behrenfeld, M. J. Gross and net primary production in the global ocean: An ocean color remote sensing perspective. *Earth-Science Reviews* **237**, 104322 (2023). URL <http://dx.doi.org/10.1016/j.earscirev.2023.104322>.
- [70] Wiggert, J. D. *et al.* The northeast monsoon’s impact on mixing, phytoplankton biomass and nutrient cycling in the arabian sea. *Deep Sea Research Part II: Topical Studies in Oceanography* **47**, 1353–1385 (2000). URL <https://www.sciencedirect.com/science/article/pii/S0967064599001472>.

- [71] Bristow, L. A., Mohr, W., Ahmerkamp, S. & Kuypers, M. M. M. Nutrients that limit growth in the ocean. *Current Biology* **27**, R474–R478 (2017). URL <https://www.sciencedirect.com/science/article/pii/S0960982217303287>.
- [72] Browning, T. J. & Moore, C. M. Global analysis of ocean phytoplankton nutrient limitation reveals high prevalence of co-limitation. *Nature Communications* **14**, 5014 (2023). URL <https://doi.org/10.1038/s41467-023-40774-0>.
- [73] Kiang, N. Y., Siefert, J., Govindjee & Blankenship, R. E. Spectral signatures of photosynthesis. i. review of earth organisms. *Astrobiology* **7**, 222–251 (2007). URL <https://doi.org/10.1089/ast.2006.0105>.
- [74] Rivkina, E. M., Friedmann, E. I., McKay, C. P. & Gilichinsky, D. A. Metabolic activity of permafrost bacteria below the freezing point. *Applied and Environmental Microbiology* **66**, 3230–3233 (2000). URL <http://dx.doi.org/10.1128/aem.66.8.3230-3233.2000>.
- [75] Takai, K. *et al.* Cell proliferation at 122°C and isotopically heavy ch₄ production by a hyperthermophilic methanogen under high-pressure cultivation. *Proceedings of the National Academy of Sciences* **105**, 10949–10954 (2008). URL <http://dx.doi.org/10.1073/pnas.0712334105>.
- [76] Noy-Meir, I. Desert ecosystems: Environment and producers. *Annual Review of Ecology and Systematics* **4**, 25–51 (1973). URL <http://dx.doi.org/10.1146/annurev.es.04.110173.000325>.
- [77] Turbet, M. *et al.* The trappist-1 habitable atmosphere intercomparison (thai). i. dry cases—the fellowship of the gcms. *The Planetary Science Journal* **3**, 211 (2022). URL <https://dx.doi.org/10.3847/PSJ/ac6cf0>.
- [78] Hersbach, H. *et al.* Era5 monthly averaged data on single levels from 1940 to present (2023).
- [79] Hassler, B. & Lauer, A. Comparison of reanalysis and observational precipitation datasets including era5 and wfde5 (2021).
- [80] Hersbach, H. *et al.* The era5 global reanalysis. *Quarterly Journal of the Royal Meteorological Society* **146**, 1999–2049 (2020). URL <http://dx.doi.org/10.1002/qj.3803>.
- [81] Bar-On, Y. M., Phillips, R. & Milo, R. The biomass distribution on earth. *Proceedings of the National Academy of Sciences* **115**, 6506–6511 (2018). URL <http://dx.doi.org/10.1073/pnas.1711842115>.
- [82] Bar-On, Y. M. & Milo, R. The biomass composition of the oceans: A blueprint of our blue planet. *Cell* **179**, 1451–1454 (2019). URL <https://doi.org/10.1016/j.cell.2019.11.018>. Doi: 10.1016/j.cell.2019.11.018.

- [83] Didan, K. Modis/terra vegetation indices monthly l3 global 0.05deg cmg v061 (2021).
- [84] Sathyendranath, S. *et al.* An ocean-colour time series for use in climate studies: The experience of the ocean-colour climate change initiative (oc-cci). *Sensors* **19**, 4285 (2019). URL <http://dx.doi.org/10.3390/s19194285>.
- [85] Rayner, N. A. *et al.* Global analyses of sea surface temperature, sea ice, and night marine air temperature since the late nineteenth century. *Journal of Geophysical Research: Atmospheres* **108** (2003). URL <https://agupubs.onlinelibrary.wiley.com/doi/abs/10.1029/2002JD002670>.
- [86] Titchner, H. A. & Rayner, N. A. The met office hadley centre sea ice and sea surface temperature data set, version 2: 1. sea ice concentrations. *Journal of Geophysical Research: Atmospheres* **119**, 2864–2889 (2014). URL <https://agupubs.onlinelibrary.wiley.com/doi/abs/10.1002/2013JD020316>.
- [87] Hague, M. & Vichi, M. Southern ocean biogeochemical argo detect under-ice phytoplankton growth before sea ice retreat. *Biogeosciences* **18**, 25–38 (2021). URL <https://bg.copernicus.org/articles/18/25/2021/>.
- [88] Randelhoff, A. *et al.* Arctic mid-winter phytoplankton growth revealed by autonomous profilers. *Science Advances* **6**, eabc2678 (2020). URL <https://doi.org/10.1126/sciadv.abc2678>.
- [89] Johnson, K. S. & Bif, M. B. Constraint on net primary productivity of the global ocean by argo oxygen measurements. *Nature Geoscience* **14**, 769–774 (2021). URL <http://dx.doi.org/10.1038/s41561-021-00807-z>.
- [90] Ryan-Keogh, T. J., Thomalla, S. J., Chang, N. & Moalusi, T. A new global oceanic multi-model net primary productivity data product. *Earth System Science Data* **15**, 4829–4848 (2023). URL <http://dx.doi.org/10.5194/essd-15-4829-2023>.
- [91] Huete, A. *et al.* Overview of the radiometric and biophysical performance of the modis vegetation indices. *Remote Sensing of Environment* **83**, 195–213 (2002). URL <https://www.sciencedirect.com/science/article/pii/S0034425702000962>. The Moderate Resolution Imaging Spectroradiometer (MODIS): a new generation of Land Surface Monitoring.
- [92] Saba, V. S. *et al.* An evaluation of ocean color model estimates of marine primary productivity in coastal and pelagic regions across the globe. *Biogeosciences* **8**, 489–503 (2011). URL <https://bg.copernicus.org/articles/8/489/2011/>.
- [93] Chatterjee, R., Singh, N., Thapa, S., Sharma, D. & Kumar, D. Retrieval of land surface temperature (lst) from landsat tm6 and tirs data by single channel

- radiative transfer algorithm using satellite and ground-based inputs. *International Journal of Applied Earth Observation and Geoinformation* **58**, 264–277 (2017). URL <http://dx.doi.org/10.1016/j.jag.2017.02.017>.
- [94] Phillips, L., Hansen, A. & Flather, C. Erratum to “evaluating the species energy relationship with the newest measures of ecosystem energy: Ndvi versus modis primary production” [remote sens. environ. 112(9) 3538–3549]. *Remote Sensing of Environment* **112**, 4380–4380 (2008). URL <http://dx.doi.org/10.1016/j.rse.2008.08.001>.
- [95] Wang, L. *et al.* Climate, topography and anthropogenic effects on desert greening: A 40-year satellite monitoring in the tengger desert, northern china. *CATENA* **209**, 105851 (2022). URL <http://dx.doi.org/10.1016/j.catena.2021.105851>.
- [96] Defries, R. S. & Townshend, J. R. G. NDVI-derived land cover classifications at a global scale. *International Journal of Remote Sensing* **15**, 3567–3586 (1994). URL <https://doi.org/10.1080%2F01431169408954345>.
- [97] Antoine, D., André, J. & Morel, A. Oceanic primary production: 2. estimation at global scale from satellite (coastal zone color scanner) chlorophyll. *Global Biogeochemical Cycles* **10**, 57–69 (1996). URL <http://dx.doi.org/10.1029/95gb02832>.
- [98] Cornec, M. *et al.* Deep chlorophyll maxima in the global ocean: Occurrences, drivers and characteristics. *Global Biogeochemical Cycles* **35** (2021). URL <http://dx.doi.org/10.1029/2020gb006759>.
- [99] Hardman-Mountford, N. J., Hirata, T., Richardson, K. A. & Aiken, J. An objective methodology for the classification of ecological pattern into biomes and provinces for the pelagic ocean. *Remote Sensing of Environment* **112**, 3341–3352 (2008). URL <http://dx.doi.org/10.1016/j.rse.2008.02.016>.
- [100] Irwin, A. J. & Oliver, M. J. Are ocean deserts getting larger? *Geophysical Research Letters* **36** (2009). URL <http://dx.doi.org/10.1029/2009gl039883>.
- [101] Mignot, A. *et al.* Understanding the seasonal dynamics of phytoplankton biomass and the deep chlorophyll maximum in oligotrophic environments: A bio-argo float investigation. *Global Biogeochemical Cycles* **28**, 856–876 (2014). URL <http://dx.doi.org/10.1002/2013gb004781>.
- [102] Druon, J.-N. *et al.* Satellite-based indicator of zooplankton distribution for global monitoring. *Scientific Reports* **9**, 4732 (2019). URL <https://doi.org/10.1038/s41598-019-41212-2>.
- [103] Hirata, T. *et al.* Synoptic relationships between surface chlorophyll-a and diagnostic pigments specific to phytoplankton functional types. *Biogeosciences* **8**,

- 311–327 (2011). URL <https://bg.copernicus.org/articles/8/311/2011/>. BG.
- [104] Longhurst, A. Seasonal cycles of pelagic production and consumption. *Progress in Oceanography* **36**, 77–167 (1995). URL <https://www.sciencedirect.com/science/article/pii/0079661195000151>.
- [105] Moudrý, V. & Devillers, R. Quality and usability challenges of global marine biodiversity databases: An example for marine mammal data. *Ecological Informatics* **56**, 101051 (2020). URL <https://www.sciencedirect.com/science/article/pii/S1574954120300017>.
- [106] Spalding, M. D., Agostini, V. N., Rice, J. & Grant, S. M. Pelagic provinces of the world: A biogeographic classification of the world’s surface pelagic waters. *Ocean & Coastal Management* **60**, 19–30 (2012). URL <http://dx.doi.org/10.1016/j.ocecoaman.2011.12.016>.
- [107] Gagné, T. O. *et al.* Towards a global understanding of the drivers of marine and terrestrial biodiversity. *PLOS ONE* **15**, e0228065 (2020). URL <http://dx.doi.org/10.1371/journal.pone.0228065>.
- [108] Pompa, S., Ehrlich, P. R. & Ceballos, G. Global distribution and conservation of marine mammals. *Proceedings of the National Academy of Sciences* **108**, 13600–13605 (2011). URL <http://dx.doi.org/10.1073/pnas.1101525108>.
- [109] Wilks, D. S. *Statistical Methods in the Atmospheric Sciences* (Academic Press, 2011).
- [110] Boers, N. *et al.* Prediction of extreme floods in the eastern central andes based on a complex networks approach. *Nature Communications* **5**, 5199 (2014). URL <https://doi.org/10.1038/ncomms6199>.
- [111] Roussel, M.-L. *et al.* Assessing the simulation of snowfall at dumont d’urville, antarctica, during the yopp-sh special observing campaign. *Quarterly Journal of the Royal Meteorological Society* **149**, 1391–1406 (2023). URL <https://rmets.onlinelibrary.wiley.com/doi/abs/10.1002/qj.4463>.
- [112] Torralba, V. *et al.* Modelling hail hazard over italy with era5 large-scale variables. *Weather and Climate Extremes* **39**, 100535 (2023). URL <https://www.sciencedirect.com/science/article/pii/S2212094722001141>.
- [113] Zhu, J., Wang, W., Liu, Y., Kumar, A. & DeWitt, D. Advances in seasonal predictions of arctic sea ice with noaa ufs. *Geophysical Research Letters* **50**, e2022GL102392 (2023).
- [114] Kim, J. & Ryu, J. H. Modeling hydrological and environmental consequences of climate change and urbanization in the boise river watershed, idaho. *JAWRA Journal of the American Water Resources Association* **55**, 133–153 (2019). URL

<https://onlinelibrary.wiley.com/doi/abs/10.1111/1752-1688.12712>.

- [115] Ma, Y., Yuan, N., Dong, T. & Dong, W. On the pacific decadal oscillation simulations in cmip6 models: A new test-bed from climate network analysis. *Asia-Pacific Journal of Atmospheric Sciences* **59**, 17–28 (2023). URL <https://doi.org/10.1007/s13143-022-00286-1>.
- [116] Ryu, Y., Berry, J. A. & Baldocchi, D. D. What is global photosynthesis? history, uncertainties and opportunities. *Remote Sensing of Environment* **223**, 95–114 (2019). URL <http://dx.doi.org/10.1016/j.rse.2019.01.016>.
- [117] Cheng, A. *et al.* Accuracy and inter-analyst agreement of visually estimated sea ice concentrations in canadian ice service ice charts using single-polarization radarsat-2. *The Cryosphere* **14**, 1289–1310 (2020). URL <https://tc.copernicus.org/articles/14/1289/2020/>.
- [118] Yang, K., Wang, Z., Deng, M. & Dettmann, B. Improved tropical deep convective cloud detection using modis observations with an active sensor trained machine learning algorithm. *Remote Sensing of Environment* **297**, 113762 (2023). URL <https://www.sciencedirect.com/science/article/pii/S0034425723003139>.
- [119] Arthur, R. & Nicholson, A. A gaian habitable zone. *Monthly Notices of the Royal Astronomical Society* **521**, 690–707 (2023). URL <https://doi.org/10.1093/mnras/stad547>.
- [120] Herbort, O., Voitke, P., Helling, C. & Zerkle, A. L. Habitability constraints by nutrient availability in atmospheres of rocky exoplanets. *International Journal of Astrobiology* **23**, e12 (2024). URL <https://www.cambridge.org/core/product/E711F9DF5EAB571E7524225AFC665AFD>.
- [121] Lehmer, O. R., Catling, D. C. & Krissansen-Totton, J. Carbonate-silicate cycle predictions of earth-like planetary climates and testing the habitable zone concept. *Nature Communications* **11**, 6153 (2020). URL <https://doi.org/10.1038/s41467-020-19896-2>.
- [122] Schulze-Makuch, D. *et al.* A two-tiered approach to assessing the habitability of exoplanets. *Astrobiology* **11**, 1041–1052 (2011). URL <https://doi.org/10.1089/ast.2010.0592>.
- [123] Copernicus Climate Change Service (C3S) Climate Data Store (CDS). Era5 monthly averaged data on single levels from 1940 to present (2023).

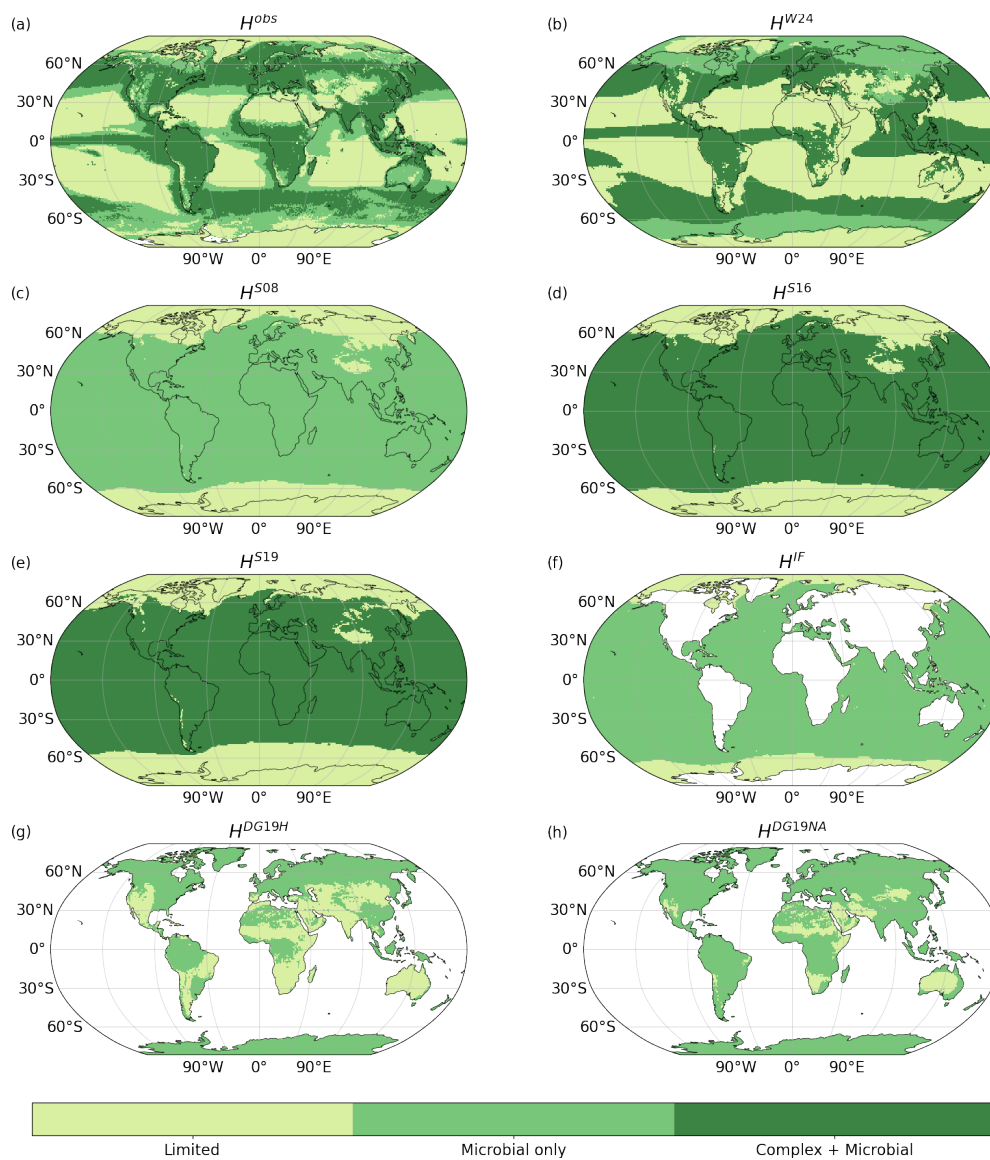


Fig. 1 The observed and metric-derived climatological surface habitability of Earth based upon the annual mean climate across 2003-2018. The habitability criteria for each metric can be found in Table 2.

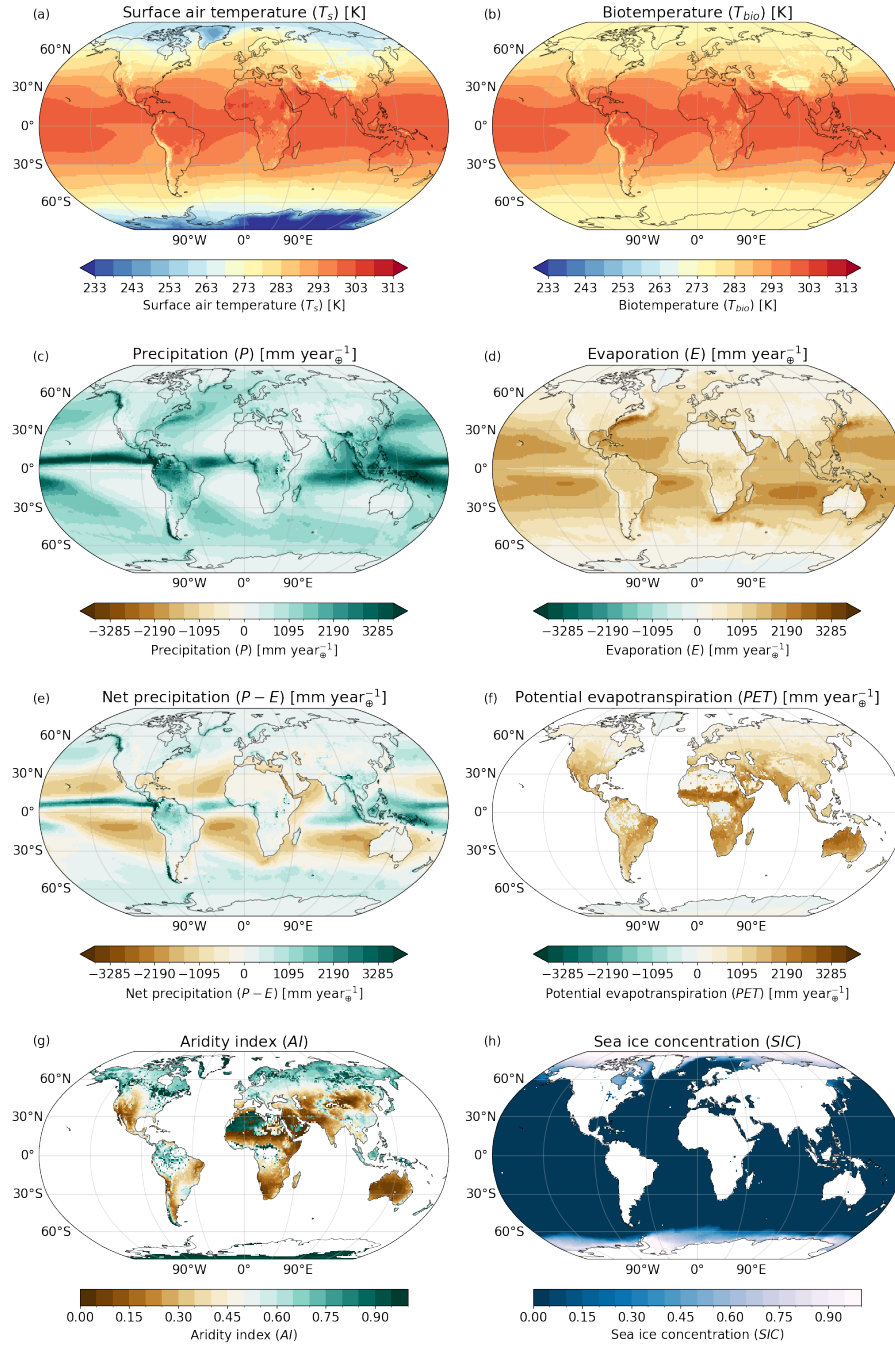


Fig. A1 Annual mean climate across 2003-2018 derived from ERA5 for (a) surface air temperature T_s [K], (b) biotemperature T_{bio} [K], (c) precipitation P [mm year^{-1}], (d) evaporation E [mm year^{-1}], (e) net precipitation $P - E$ [mm year^{-1}], (f) potential evapotranspiration PET [mm year^{-1}], (g) aridity index AI , and (h) sea ice concentration SIC .